Hindawi Publishing Corporation
Physics Research International
Volume 2011, Article ID 705686, 8 pages
doi:10.1155/2011/705686

Research Article

L X-Rays RYIED Oscillations and Proton-NMRD of Gd_2O_3 Nanoparticles

A. Taborda,[1,2] M. A. Reis,[1,2] P. C. Chaves,[1,2] and A. Carvalho[3]

[1] *Física e Unidade de Acelerador, Instituto Tecnológico e Nuclear, Estrada Nacional 10, 2686-953 Sacavém, Portugal*
[2] *Centro de Física Atómica da Universidade de Lisboa, Avenida Prof. Gama Pinto 2, 1649-003 Lisboa, Portugal*
[3] *Centro de Física da Matéria Condensada da Universidade de Lisboa, Avenida Prof. Gama Pinto 2, 1649-003 Lisboa, Portugal*

Correspondence should be addressed to M. A. Reis, mareis@itn.pt

Received 17 September 2010; Revised 4 January 2011; Accepted 8 March 2011

Academic Editor: Sergey B. Mirov

Recently, it was shown that relative yields of X-rays induced by ion impact are not constant but depend on beam energy. In the framework of this problem, pellets of Gd_2O_3 and a Gd chelate, Gd-DOTA, as well as a 5 nm in diameter Gd_2O_3 nanoparticles dispersion on a polycarbonate Nuclepore filter, were studied. In this work, it is shown that after subtraction of known matrix effects, relative yield variations still present different patterns for Gd_2O_3 pellet and Gd_2O_3 nanoparticles. Proton NMRD $T_1(\omega)$ data for Gd_2O_3 nanoparticles and Gd-DOTA water solutions published by Bridot et al. and Toth et al., respectively, were reproduced using a model for paramagnetic substances in water solutions and identical electronic relaxation times. The analysis of both techniques results points collective electron behaviour as the explanation for the different observations on X-ray data of Gd_2O_3 nanoparticles and bulk material.

1. Introduction

In Particle Induced X-Ray Emission (PIXE), it is usually assumed that the ratio between two X-ray lines of the same element is an atomic parameter independent of the chemical environment surrounding the emitting ion. That this in detail is not exactly the case is also a well-known fact, shown by several authors [1–10]. Furthermore, recently, effects due to an applied external magnetic field have been reported on the fluorescence yield of L_3 sub-shell of Gd, Dy, Hg, and Pb by Demir and Şahin [11].

Taking into account that, in a PIXE experiment, the X-ray emitting ion is located in a condensed matter environment and is therefore subjected to strong local magnetic and electric fields, the result from Demir may be seen as a clear demonstration that the solid state environment may well affect electronic transition rates as well as it affects details on the valence electronic configuration of the emitting ion [8, 9]. Furthermore, it is important to realise that in parallel to the main process of ionisation of the inner-shells and first-order processes of reorganisation of the electron cloud, namely, the emission of X-rays or Auger electrons, the collision between the incident ions and the sample atoms also induces other secondary processes such as multi-ionisation, electrons shake-up and shake-off, polarisation of atomic orbitals and multiparticle and collective processes such as the emission of Radiative Auger Emission X-rays (RAE) [12, 13] and production of intrinsic and extrinsic plasmons [14, 15]. The result of all these is that the relative intensity of X-ray lines corresponding to transitions to the same subshell ends up being apparently or even in fact dependent on the chemical (or electronic) environment of the emitting ion as well as on the incident ion beam energy. This effect has been named RYIED-Relative Yield Ion Energy Dependence and has been under study by the authors since several years now [1, 16, 17].

In the case of proton Nuclear Magnetic Resonance Dispersion (NMRD), the longitudinal relaxation time T_1 and the transverse relaxation time T_2 are measured for a broad range of Larmor frequencies (ω). The obtained $T_1(\omega)$ or $T_2(\omega)$ curves are called nuclear magnetic relaxation dispersion curves, and NMRD is particularly interesting in

the study of paramagnetic and superparamagnetic systems. The fitting of the $T_1(\omega)$ curves, using appropriate models, provides an important insight into the paramagnetic centre environment [18], including also parameters relative to the paramagnetic centre itself. In a preliminary work [19], a possible resemblance between the magnetic field in NMRD experiments and the ion beam energy in RYIED, as well as between the $T_1(\omega)$ curves in NMRD and the intensity ratio variation curves in RYIED, was put forward by the first time. Taking into account, for the RYIED case, that

(i) the impact of an incident ion on a target, as well as the emission of the scattered electrons, corresponds to electromagnetic pulses,

(ii) the duration of the electromagnetic pulse corresponding to the incident ion is roughly proportional to the inverse of the speed of the impinging ion,

(iii) the ionisation of the target converts a closed, ideally momentless shell, into an asymmetric shell with a magnetic and electric moments that are not null,

(iv) the emission of an electron by an initially neutral atom generates plasmons in the material where the ion is embedded,

the links between RYIED and NMRD become clear, because the electromagnetic pulses associated to the ion beam can be seen as perturbations comparable to the RF pulses used to obtain NMRD $T_1(\omega)$ data.

Regarding NMRD data, $1/T_1(\omega)$ measures the rate at which the protons in a water solution of a magnetically active substance align with a magnetostatic field once taken out of that condition by an RF pulse in the resonance condition. Now, different X-rays correspond to different transitions of the whole ion between two different excited (ionic) states, each transition having its own characteristic partial half-life. Calculating the relative intensity of two different atomic transitions is, therefore, among other things, a way of calculating the ratio of intensity of transitions (between ionic states) that take place in two different times after collision. This is much the same as saying that it is a way to measure the rate at which beam-induced ion states precess, loose alignment or, are otherwise time affected by an essentially nonsymmetric electrostatic and magnetostatic local field and other electronic collective phenomena, in a close similarity to $1/T_1(\omega)$ measurements. Furthermore, it is here quite important to realise that what controls atomic processes is the combination of fields and not the classical positions of atomic or molecular electrons. Since changes in sources of fields (e.g., the ionisation process) propagate at the speed of light and not at the speed of electrons or protons, in detail the whole process should not be seen as frozen relative to the protons speed, as usually it is.

In the present paper, it is shown that a similarity observed between NMRD curves for the Gd chelate Gd-DOTA and Gd_2O_3 nanoparticles solutions and similarities observed between Gd-DOTA and Gd_2O_3 nanoparticles in RYIED can be explained by a similarity between effective values for the longitudinal and transverse electronic spin relaxation times of Gd electrons in both environments, a result that strongly supports both the above stated view upon the resemblance between RYIED and proton NMRD, as well as the existence of a collective behaviour of electrons in Gd_2O_3 nanoparticles, different from those present in bulk pressed powder Gd_2O_3 pellets.

2. Materials and Methods

After studying the relative intensity variations on W and Mo L X-rays in previous works [1, 2, 17], a decision was made to study an element allowing the easy measurement of the L shell as well as the K and the M shells X-rays. Gd was selected, among other reasons also because Gd is an important technological element, namely, for biomedical applications, being used as paramagnetic contrast agent (CA) for nuclear magnetic resonance imaging (MRI), due to its large magnetic moment [20]. Regarding RYIED, Gd L-shell spectra were obtained using a Gresham Scientific Instruments Lda 150 eV resolution LN-cooled Scirus Si(Li) detector. As irradiation targets, a Gd_2O_3 pellet, a Gd_2O_3 5 nm particles dispersion on a polycarbonate membrane filter, and a Gd-DOTA pellet were used. Gd-DOTA (gadolinium-tetraazacyclododecanetetraacetic acid complex) is a Gd chelate used in the production of MRI contrast agents [21]. Pure materials, namely, 99.99% pure Gd_2O_3 powder from Alfa Aeser and 99.9% pure Gd_2O_3 nanoparticles and 97.5% pure Gd-DOTA from Sigma-Aldrich Co., were used to avoid problems in data interpretation due to sample contamination. Further, to avoid problems due to the sample preparation, irradiation targets were made in a glove chamber and in an inert dry atmosphere to prevent for sample degradation. Once ready, the samples were placed in the irradiation chamber under vacuum, to assure that no degradation or contamination would arise from atmospheric exposure, which was thus limited to a very few minutes necessary for closure and evacuation of the irradiation chamber. The experimental facilities details can be found elsewhere [22]. High statistics spectra were collected (roughly 200 000 counts in the L_α) for proton energies from 700 keV to 1450 keV in steps of 50 keV, and for 1700 keV and 1950 keV. Spectra deconvolution was carried out using the new DT2 program fitting core [23]. This includes a Bayesian inference algorithm by Barradas [24], for determination of the error levels associated to the fitted line areas. The precision of the Bayesian inference algorithm plays an important role in this work, allowing for errors below 5% in most cases.

A Python routine specifically written for the purpose was used to calculate the experimental line intensity ratios. The theoretical values of X-ray line intensities and intensity ratios were calculated using the C calculation routine DT2simul [25].

The NMRD data for the gadolinium oxide nanoparticles of three different sizes was obtained from the work of Bridot et al. [26]. Data for the Gd-DOTA was obtained from the work of Toth et al. [20]. The $1/T_1(\omega)$ data fitting was performed using the commercial software SigmaPlot.

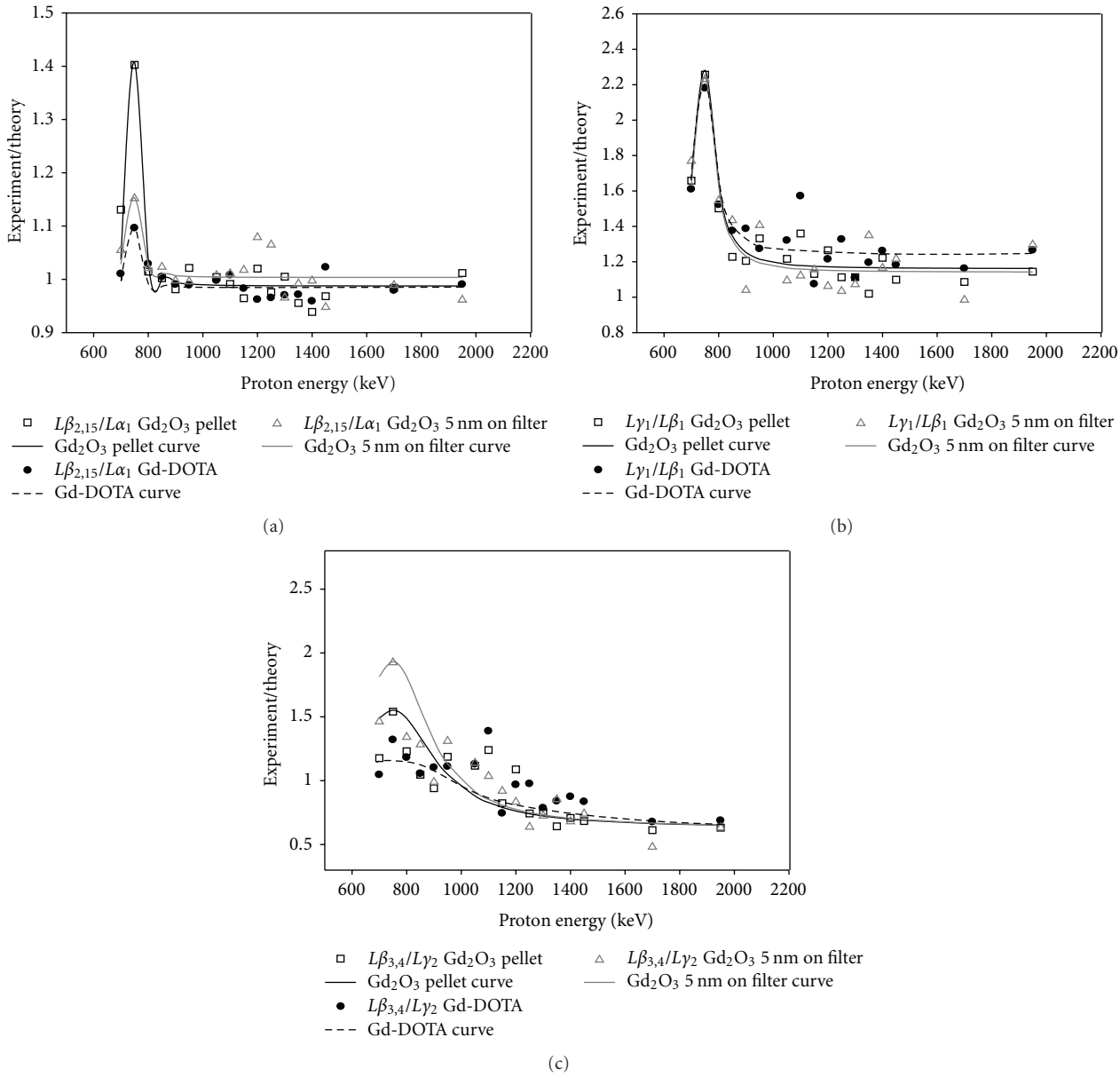

FIGURE 1: $L\beta_{2,15}/L\alpha_1$, $L\gamma_1/L\beta_1$, and $L\beta_{3,4}/L\gamma_2$ line intensity ratios normalised to the theoretical values, obtained using DT2simul, for the Gd_2O_3 pellet, the Gd_2O_3 5 nm on filter, and the Gd-DOTA samples as a function of proton energy.

3. Results and Discussion

3.1. RYIED. Figure 1 shows the ratios of intensity determined for lines corresponding to transitions to the same sub-shell, namely, $L\beta_{2,15}/L\alpha_1(L_3N_{4,5}/L_3M_5)$, $L\gamma_1/L\beta_1(L_2N_4/L_2M_4)$, and $L\beta_{3,4}/L\gamma_2(L_1M_{2,3}/L_1N_2)$, for the three different Gd environments, and as function of the incident proton beam energy, after being normalised to the expected theoretical values.

It can be seen that the intensity ratios variation curves obtained are different not only for the three samples: the Gd-DOTA pellet, the Gd_2O_3 5 nm particles dispersed on a filter, and the Gd_2O_3 pellet, but more than that, the experimental ratios are significantly different from the theoretical expectations, mainly at low energy. Apart from the amplitude, the oscillations seen are not new and were observed in previous works on the K X-rays RYIED of a Gd_2O_3 pellet sample [17] as well as in studies made on L and K X-rays of Mo [2, 16, 17] and W samples [1, 16, 27].

Figure 1, nevertheless, presents a very surprising result. The patterns obtained for the Gd_2O_3 pellet and the Gd_2O_3 5 nm particles are different. This is a striking result because it means that the oscillating pattern is not only dependent on the local chemical composition (which is the same for the pellet and for the nanoparticles), but also in some property related to the size of the nanoparticles. It is important to realise here that "normal" matrix effects are already excluded by normalisation to theoretical (simulated) values, which

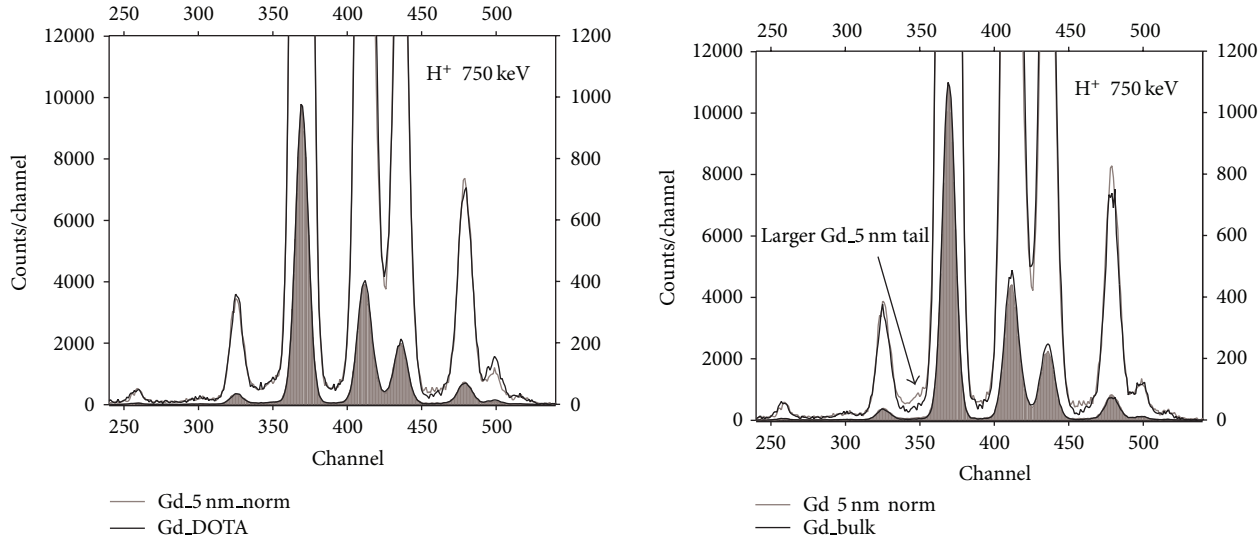

Figure 2: Overlap of spectra collected during irradiation of Gd_2O_3 nanoparticles, Gd-DOTA pellets (a), and Gd_2O_3 powder pellets (b), using 750 keV proton beams. The Gd_2O_3 nanoparticles spectrum was normalised in order that the peak counts in the $L\alpha$ peak are the same as that of the overlapping spectra. It can be seen that while the tail region of the $L\alpha$ peak is identical for the Gd_2O_3 nanoparticles and for the Gd-DOTA pellet, the same is not true for the Gd_2O_3 nanoparticles and the Gd_2O_3 bulk pellet.

include these "normal" effects [28, 29]. The second amazing result in Figure 1 is the resemblance between the patterns for the Gd_2O_3 5 nm particles and those for the Gd-DOTA pellet, in the $L\beta_{2,15}/L\alpha_1$ plot.

The question is what resemblance can be found between Gd_2O_3 5 nm particles and a Gd-DOTA chelate that may justify these results. One detail that can be observed is the fact that in all ratios, one of the transitions considered involves electrons originating from the N-shell and, therefore, close enough to the valence shell of Gd.

Finally, it is important to realise that all these ratios correspond to ratios between transitions to the same L subshell (as pointed out initially), and therefore conditions such as strong variations in the L_3/L_1 ionisation cross-section ratios do not apply here.

Since the most striking result is observed for the 750 keV irradiations, some specific attention may be put into these spectra. In Figure 2, the overlap of Gd_2O_3 nanoparticles spectra and those of Gd-DOTA (top graph) and Gd_2O_3 powder pellet (bottom graph) are presented. Gd_2O_3 nanoparticles spectra were normalised to the others to simplify the comparison.

In the case of the overlap with the Gd-DOTA spectra, the similitude is such that if it were not for the differences in the $L\gamma$ group around channel 500, it could be thought that the spectra were the same. This is definitely not seen in the overlap with the Gd_2O_3 powder pellet spectrum, since the low-energy tail region is impressively different. Furthermore, and strange enough, the highest tail corresponds to the Gd_2O_3 nanoparticles and not to the powder pellet.

Since the low energy tail may contain contributions from Radiative Auger Emission (RAE) satellites [12, 13] as well as other satellites due to collective electron behaviours [14, 15], this is another result suggesting that collective or second-order phenomena may be behind the strange results displayed in Figure 1.

3.2. NMRD. Turning now to NMRD, Figure 3 shows the comparison of the longitudinal relaxivity data from water solutions of Endorem [30], Gd-DOTA [20], and three different sizes of functionalized Gd_2O_3 nanoparticles [26].

Endorem (or AMI-25) and Gd-DOTA are contrast agents used in Magnetic Resonance Imaging (MRI). Endorem (or AMI-25) is an aqueous colloidal suspension of superparamagnetic iron oxide (Fe_2O_3 and Fe_3O_4 mixture) nanoparticles, while Gd-DOTA is a paramagnetic chelate.

Paramagnetic and superparamagnetic contrast agents are expected to have strikingly different signatures in the nuclear magnetic resonance dispersion profiles as shown in Figure 3 for Endorem and Gd-DOTA.

Given that Gd_2O_3 is a material expected to have a specific magnetic moment higher than Fe_2O_3 or Fe_3O_4, the Gd_2O_3 nanoparticles NMRD $1/T_1(\omega)$ curves should at first behave like Endorem and not like Gd-DOTA. Still, as shown in Figure 3, they do behave like Gd-DOTA for Larmor frequencies between 0.01 MHz and 100 MHz. Furthermore, as stated by Bridot et al. [26], the magnetic behaviour of these gadolinium oxide nanoparticles is not yet fully elucidated. Now, given the resemblance between the NMRD curves of Gd_2O_3 nanoparticles and Gd-DOTA, as well as RYIED patterns, one may consider that, in the range of proton Larmor frequencies of interest, Gd_2O_3 nanoparticles behave like a paramagnetic substance in respect to their effect on nuclear relaxation of water protons.

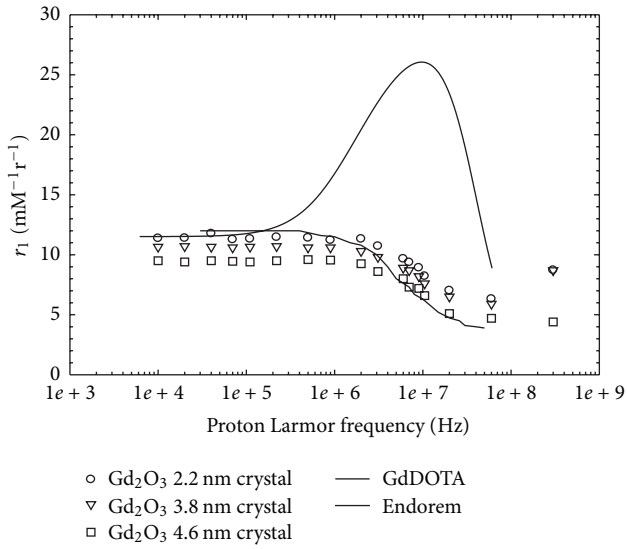

FIGURE 3: Comparison of the longitudinal relaxivity (defined in (2)) as a function of proton Larmor frequency between the three sizes of gadolinium oxide (Gd_2O_3) nanoparticles [26], a superparamagnetic nanoparticles suspension (Endorem) [30], and a paramagnetic chelates solution (Gd-DOTA) [20].

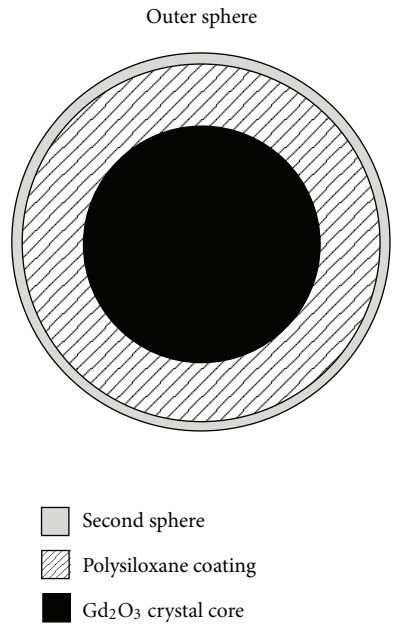

FIGURE 4: Schematic illustration of the Gd_2O_3 nanoparticles model considered. The thin layer on top of the Polysiloxane shell is considered to be the second sphere. The outer sphere is considered as fully outside to the particles structure.

3.2.1. Theoretical Approach. The use of the theory of solvent nuclear relaxation in the presence of paramagnetic substances developed by Bloembergen [31], Solomon [32], and others was therefore considered in its version specially developed for studying the effect of paramagnetic chelates in water relaxation [20]. Here it is important to realise that the system to be studied is not a single paramagnetic ion surrounded by a molecule (a chelate) but instead a Gd_2O_3 crystal core coated with a 2 nm Polysiloxane shell [26], as presented schematically in Figure 4.

This leads to two important facts.

(i) Water protons do not have access to sites near the Gd core, the inner sphere in the Bloembergen-Solomon model, and therefore only the second- and outer-sphere terms may be considered, making the longitudinal relaxation rate be given by [20]

$$\frac{1}{T_1} = \left(\frac{1}{T_1}\right)^{2\text{nd}} + \left(\frac{1}{T_1}\right)^{\text{OS}}, \tag{1}$$

$$\frac{1}{T_1} = r_1[M] + \left(\frac{1}{T_1}\right)_{\text{medium}}, \tag{2}$$

where r_1 is the longitudinal relaxivity, $[M]$ is the concentration of the paramagnetic element (in this case Gd), and $(1/T_1)_{\text{medium}}$ is the longitudinal relaxation rate of the medium where the paramagnetic chelates are suspended.

(ii) There is a need to consider a set of effective terms by assuming both a pure mechanical spherical symmetry of the particle and a coherent, or at least highly correlated, collective behaviour of the Gd_2O_3 nanoparticles electrons.

The second-sphere term, $(1/T_1)^{2\text{nd}}$, can be expressed as [20]

$$\left(\frac{1}{T_1}\right)^{2\text{nd}} = P_m \sum_{j=1}^{N_{\text{H2O}}} \frac{1}{T_{1,j} + \tau_{m,j}}, \tag{3}$$

where P_m is the mole fraction of bound water nuclei in the second-sphere, with N_{H2O} being the number of specially bound water molecules in the second-sphere, $\tau_{m,j}$ the lifetime of a specific water molecule j in the second shell, and $1/T_{1,j}$ the longitudinal proton relaxation rate of molecule j for water protons in the second sphere.

Assuming a spherical symmetry geometry for the particles leads to the definition of effective parameters and to rewriting (3) as

$$\left(\frac{1}{T_1}\right)^{2\text{nd}} = \frac{cN}{T_1^{\text{eff}} + \tau_m^{\text{eff}}}, \tag{4}$$

where $N = qN_{\text{H2O}}/55.5$, with q being the number of bound water nuclei per Gd and c the molal concentration of the paramagnetic element. T_1^{eff} is assumed to be given by

$$\frac{1}{T_1^{\text{eff}}} = \frac{2}{15}\left(\frac{\gamma_I^2 g^2 \mu_B^2}{r_{\text{GdH}}^6}\right) S(S+1)\left(\frac{\mu_0}{4\pi}\right)^2 \times \left(7\frac{\tau_{c2}}{1+\omega_S^2\tau_{c2}^2} + 3\frac{\tau_{c1}}{1+\omega_I^2\tau_{c1}^2}\right), \tag{5}$$

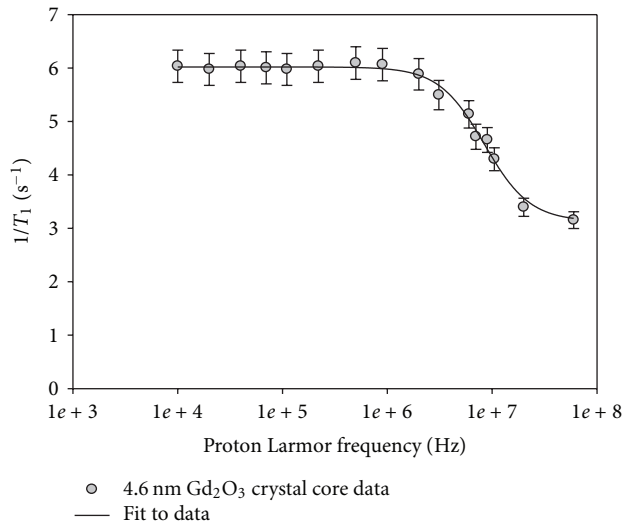

Figure 5: Longitudinal relaxation rates as a function of proton Larmor frequency and fitting curve to the 4.6 nm diameter Gd_2O_3 crystal core nanoparticles data from Bridot et al. [26] using the paramagnetic model of nuclear relaxation described above.

where the subscript I refers to the water proton nuclear spin and the subscript S refers to the gadolinium nanoparticle electron spin. All the parameters in the right-hand side of the equation are to be taken as effective parameters.

In (5), the following was considered: (1) r_{GdH} is the distance between the water proton and the centre of the crystal core, (2) S was assumed to be $198\,\mu_B$ by considering a spin density of $3.86\,\mu_B/\mathrm{nm}^3$, calculated from a lattice constant of 1.0812 nm determined by Niinistö for a cubic body-centred crystalline structure Gd_2O_3 nanoparticles [33], (3) the τ_{ck} are effective times characteristic of relaxation times defined as

$$\frac{1}{\tau_{ck}} = \frac{1}{\tau_R} + \frac{1}{T_{ke}} + \frac{1}{\tau_m^{\mathrm{eff}}}, \tag{6}$$

$k = 1, 2$, where the right hand terms are effective values for the rotational correlation time τ_R, the longitudinal and transverse electron spin relaxation times of Gd, T_{1e} and T_{2e}, respectively, and τ_m^{eff} the mean lifetime of a water molecule in the second-sphere, (4) based on the similarity between the Gd_2O_3 nanoparticles response and that of Gd-DOTA for both NMRD and RYIED, it was decided to take, as effective electronic relaxation times, the electronic relaxation times determined by Powell et al. [34] for Gd-DOTA: $T_{1e} = 5.0 \times 10^{-10}$ s and $T_{2e} = 1.08 \times 10^{-9}$ s.

Finally, for the outer-sphere term, the last term in (1), is given as in [20] and is written as

$$\left(\frac{1}{T_1}\right)^{\mathrm{OS}} = \frac{32\pi}{405}\left(\frac{\mu_0}{4\pi}\right)^2 \frac{N_A[M]}{dD}\gamma_I^2\gamma_S^2\hbar S(S+1) \times \left[j_2(\omega_I - \omega_S) + 3j_1(\omega_I) + 6j_2(\omega_I + \omega_S)\right], \tag{7}$$

Table 1: Fitting parameters for the 4.6 nm diameter Gd_2O_3 crystal core nanoparticles and for the Gd-DOTA chelates found in the literature [34].

Parameters	Gd_2O_3	Gd-DOTA [34]
r_{GdH}(m)	7.58×10^{-9}	3.1×10^{-10}
τ_R (s)	1.71×10^{-9}	7.7×10^{-11}
τ_m^{eff} (s)	2.47×10^{-10}	2.4×10^{-7}
N	5.73	—
D (m^2/s)	6.0×10^{-10}	2.2×10^{-9}
d (m)	1.2×10^{-8}	$> r_{\mathrm{GdH}}$
T_{1e} (s)	5.0×10^{-10}	5.0×10^{-10}
T_{2e} (s)	1.08×10^{-9}	1.08×10^{-9}

where $j_k(\omega)$ are spectral density functions [35] given in this case by

$$j_k(\omega) = \mathrm{Ree}\left(\frac{1 + z/4}{1 + z + 4z^2/9 + z^3/9}\right) \tag{8}$$

with $z = \sqrt{i\omega\tau + \tau/T_{\mathrm{ke}}}$, $\tau = d^2/D$, and $k = 1, 2$.

The diffusion coefficient for relative diffusion D was taken equal to the one obtained for Endorem in a previous work [30, 36], since Gd_2O_3 nanoparticles may be seen as mechanically similar to Endorem nanoparticles. The distance of closest approach of the Gd electron spin and the water proton spin in the outer-sphere d was fitted assuming that it could not be smaller than the hydrodynamic radius of the nanoparticles, namely, 8.9 nm for the nanoparticles with a crystal core of 4.6 nm [26]. This value was also considered as a rough value for r_{GdH} for fitting the d parameter. Once the value for d is obtained, the following parameters for the second sphere were fitted: r_{GdH}, τ_R, τ_m^{eff}, and N.

3.2.2. NMRD Curves and Fitting Results. Figure 5 presents the experimental NMRD data for the Gd_2O_3 nanoparticles [26] as well as the results of the fit of (1) to these. The experimental longitudinal relaxation rates data, $1/T_1$, shown in Figure 5, for the nanoparticles with a Gd_2O_3 crystal core having a diameter of 4.6 nm, were calculated from the r_1 values in Bridot et al. [26] using the known relation between relaxation rates and relaxivity expressed in (2). The medium was assumed to be water at 25°C, $(1/T_1)_{\mathrm{medium}} \approx 0.333\,\mathrm{s}^{-1}$, and the concentration of gadolinium, $[M]$, was taken as 0.6 mM based on the information in page 5079 of [26].

It can be seen that the fitted curve follows closely the experimental points extracted from the literature.

The fitted values for the model parameters are shown in Table 1. Errors associated with these are not presented because they are irrelevant for the present discussion. In fact, what this result points out is that, by using the electronic longitudinal and transverse relaxation times of Gd-DOTA as effective electronic longitudinal and transverse relaxation times of the Gd_2O_3 nanoparticles, it is possible to reproduce its NMRD experimental data, which is a valid result, independent of the precision of the values obtained for the fitting parameters.

4. Summary and Conclusions

This last result in the previous section shows that electrons in Gd_2O_3 nanoparticles present an effective electronic relaxation behaviour identical to that reported in the literature for Gd-DOTA electrons. On the other hand, RYIED oscillation patterns for Gd-DOTA and for Gd_2O_3 nanoparticles also show a very similar structure for a ratio involving the valence transitions $L\beta_{2,15}$. Besides, the low energy tail of spectra collected during irradiations at the ion beam energy where this effect is more striking also points out to a similar electronic behaviour at an atomic or nanoparticle scale. The conjugation of all these results allows us to conclude that RYIED oscillation patterns are most probably linked to collective electronic properties of materials under analysis either directly or through its effect on second-order phenomena. In fact, in the case of Gd_2O_3 nanoparticles, the existence of a collective coherent behaviour is clearly compatible with the NMRD curves, and, in the case of the RYIED and spectra resemblances (and differences) for the most critical ion beam energy, results are also strongly in favour of this interpretation.

The possibility of accessing information regarding electronic collective behaviour in materials such as Gd_2O_3 nanoparticles is a very important result since this is an information hard to access and frequently only available by the use of large infrastructures whoes effective beam time available is always limited. In the specific case of Gd, the importance is enhanced due to its relevance in technological applications, namely, for biomedical applications such as paramagnetic contrast agent in nuclear magnetic resonance imaging (MRI), or even as a possible basis for therapeutic methodologies under development (like diathermy therapy). The preliminary results here reported should thus lead to further studies allowing a complete clarification of the full potential of the present analytical approach, part of which should include high-resolution X-rays spectrometry using either standard crystal spectrometers of, preferably, microcalorimeter EDS detectors, in order to be able to resolve low energy tail contributions [37] and thus become in possession of better and richer X-ray data that is not strongly affected by the detectors response function.

The holistic analysis of X-ray and NMRD data is also of the utmost importance both for a positive demonstration that electrons collective behaviour is indeed affecting X-ray data, as well as for robustness of the analysis of unknown samples, once the above demonstration has been achieved.

Acknowledgments

The authors are grateful to J. P. Leal for making available the use of the glove chamber and for his help in its operation. The proficient collaboration of Ms. Rute Pinheiro in helping with sample preparation detailed procedures is also acknowledged. The present work was partially funded by the Fundação para a Ciência e a Tecnologia through contracts REEQ/377/FIS/2005, SFRH/BD/27557/2006, and SFRH/BD/43379/2008.

References

[1] M. A. Reis, P. C. Chaves, and J. C. Soares, "Particle induced X-ray emission—relative yield ion energy dependence, an IBA chemical speciation method," *Nuclear Instruments and Methods in Physics Research B*, vol. 229, no. 3-4, pp. 229–413, 2005.

[2] P. C. Chaves and M. A. Reis, "Comparative study of W-K and L shells relative yield ion energy dependence," in *Proceedings of the 10th International Conference on Particle Induced X-Ray Emission and Its Analytical Applications*, M. Budnar and M. Kavčič, Eds., p. 810.1, 2004, Digitally Published.

[3] S. Raj, H. C. Padhi, and M. Polasik, "Influence of chemical effect on the Kβ-to-Kα X-ray intensity ratios of Ti, V, Cr and Fe in TiC, VC, CrB, CrB and FeB," *Nuclear Instruments and Methods in Physics Research B*, vol. 145, no. 4, pp. 485–491, 1998.

[4] S. Raj, H. C. Padhi, and M. Polasik, "Influence of alloying effect on Kβ/Kα X-ray intensity ratios of V and Ni in V_xNi_{1-x} alloys," *Nuclear Instruments and Methods in Physics Research B*, vol. 155, no. 1, pp. 143–152, 1999.

[5] S. Raj, H. C. Padhi, D. K. Basa, M. Polasik, and F. Pawlowski, "Kβ-to-Kα X-ray intensity ratio studies on the changes of valence electronic structures of Ti, V, Cr, and Co in their disilicide compounds," *Nuclear Instruments and Methods in Physics Research B*, vol. 152, no. 4, pp. 417–424, 1999.

[6] S. Raj, H. C. Padhi, and M. Polasik, "Influence of chemical effect on the Kβ-to-Kα X-ray intensity ratios of Cr, Mn and Co in CrSe, MnSe, MnS and CoS," *Nuclear Instruments and Methods in Physics Research B*, vol. 160, no. 4, pp. 443–448, 2000.

[7] H. C. Padhi, C. R. Bhuinya, and B. B. Dhal, "Influence of solid-state effects on the Kβ/Kα intensity ratios of Ti and V in TiB, VB and VN," *Journal of Physics B*, vol. 26, no. 23, pp. 4465–4469, 1993.

[8] F. Pawlowski, M. Polasik, S. Raj, H. C. Padhi, and D. K. Basa, "Valence electronic structure of Ti, Cr, Fe and Co in some alloys from Kβ-to-Kα X-ray intensity ratio studies," *Nuclear Instruments and Methods in Physics Research B*, vol. 195, no. 3-4, pp. 367–373, 2002.

[9] K. Jankowski and M. Polasik, "On the calculation of $K\beta/K\alpha$ X-ray intensity ratios," *Journal of Physics B*, vol. 22, no. 15, pp. 2369–2376, 1989.

[10] K. Kawatsura, K. Ozawa, M. Terasawa, K. Komaki, and F. Fujimoto, "Computer simulationof channeling implantation at high and medium energies," *Nuclear Instruments and Methods in Physics Research B*, vol. 75, pp. 28–32, 1993.

[11] D. Demir and Y. Şahin, "The effect of an external magnetic field on the L3 subshell fluorescence yields and level widths for Gd, Dy, Hg and Pb at 59.5 keV," *Nuclear Instruments and Methods in Physics Research B*, vol. 254, no. 1, pp. 43–48, 2007.

[12] F. Bloch and P. A. Ross, "Radiative auger effect," *Physical Review*, vol. 47, no. 11, pp. 884–885, 1935.

[13] M. C. Lépy, J. Plagnard, and J. Morel, "Radiative Auger effect: an explanation for discrepancies between theoretical and experimental $K\beta/K\alpha$ X-ray emission probability ratios?" *Nuclear Instruments and Methods in Physics Research A*, vol. 339, no. 1-2, pp. 241–247, 1994.

[14] D. C. Langreth, "Born-oppenheimer principle in reverse: electrons, photons, and plasmons in solids-singularities in their spectra," *Physical Review Letters*, vol. 26, no. 20, pp. 1229–1233, 1971.

[15] R. W. Ditchfield, "Measurement and interpretation of the plasmon energy in alumina," *Solid State Communications*, vol. 19, no. 5, pp. 443–444, 1976.

[16] P. C. Chaves, M. A. Reis, N. P. Barradas, and M. Kavčič, "Dependence of relative intensity of L1 sub-shell X-rays on ion beam energy," *Nuclear Instruments and Methods in Physics Research B*, vol. 261, no. 1-2, pp. 121–124, 2007.

[17] P. C. Chaves, M. Reis, and E. Alves, "New high energy and high resolution lisbon PIXE set-up," in *Proceedings of the 11th International Conference on PIXE and Its Analytical Applications*, J. Miranda, J. L. Rucalva-Sil, and O. G. de Lucio, Eds., pp. PII-2-1–PII-2-4, 2007.

[18] L. Helm, "Relaxivity in paramagnetic systems: theory and mechanisms," *Progress in Nuclear Magnetic Resonance Spectroscopy*, vol. 49, no. 1, pp. 45–64, 2006.

[19] M. A. Reis, P. C. Chaves, A. Taborda, and A. Carvalho, "Comparison of Gd L-Xrays RYIED and proton NMRD," in *Proceedings of the 11th International Conference on PIXE and Its Analytical Applications*, J. Miranda, J. L. Rucalva-Sil, and O. G. de Lucio, Eds., p. PI-6, 2007.

[20] E. Toth, L. Helm, and A. E. Merbach, "Relaxivity of gadolinium(III) complexes: theory and mechanism," in *The Chemistry of Contrast Agents in Medical Magnetic Resonance Imaging*, E. Toth and A. E. Merbach, Eds., John Wiley & Sons, New York, NY, USA, 2001.

[21] J. C. Bousquet, S. Saini, D. D. Stark et al., "Gd-DOTA: characterization of a new paramagnetic complex," *Radiology*, vol. 166, no. 3, pp. 693–698, 1988.

[22] M. A. Reis, P. C. Chaves, V. Corregidor et al., "Detection angle resolved PIXE and the equivalent depth concept for thin film characterization," *X-Ray Spectrometry*, vol. 34, no. 4, pp. 372–375, 2005.

[23] M. A. Reis, P. C. Chaves, L. C. Alves, and N. P. Barradas, "Dt2, a pixe spectra simulation and fitting package," *X-Ray Spectrometry*, vol. 37, no. 2, pp. 100–102, 2008.

[24] N. P. Barradas and C. Jeynes, "Advanced physics and algorithms in the IBA DataFurnace," *Nuclear Instruments and Methods in Physics Research B*, vol. 266, no. 8, pp. 1875–1879, 2008.

[25] A. Taborda, P. C. Chaves, and M. A. Reis, "Universal polynomial approximation to crosssections of K- and L-shell ionisation induced by H and He ion beams," *X-Ray Spectrometry*, vol. 40, no. 3, pp. 127–134, 2011.

[26] J. L. Bridot, A. C. Faure, S. Laurent et al., "Hybrid gadolinium oxide nanoparticles: multimodal contrast agents for in vivo imaging," *Journal of the American Chemical Society*, vol. 129, no. 16, pp. 5076–5084, 2007.

[27] H. Mohan and A. K. Jain, "Energy dependence of proton-induced L X-ray production cross-section for W," *Nuclear Instruments and Methods in Physics Research B*, vol. 266, no. 8, pp. 1203–1205, 2008.

[28] C. Pascual-Izarra, N. P. Barradas, and M. A. Reis, "LibCPIXE: a PIXE simulation open-source library for multilayered samples," *Nuclear Instruments and Methods in Physics Research B*, vol. 249, no. 1-2, pp. 820–822, 2006.

[29] M. A. Reis, L. C. Alvesa, and A. P. Jesus, "Matrix effects correction for quantitative TTPIXE analysis," *Nuclear Instruments and Methods in Physics Research B*, vol. 109-110, pp. 134–138, 1996.

[30] A. Taborda and A. Carvalho, "Superparamagnetic iron oxide nanoparticles—proton nuclear magnetic resonance dispersion curves," *European Physical Journal*, vol. 43, no. 2, pp. 145–148, 2008.

[31] N. Bloembergen, E. M. Purcell, and R. V. Pound, "Relaxation effects in nuclear magnetic resonance absorption," *Physical Review*, vol. 73, no. 7, pp. 679–712, 1948.

[32] I. Solomon, "Relaxation processes in a system of two spins," *Physical Review*, vol. 99, no. 2, pp. 559–565, 1955.

[33] J. Niinistö, N. Petrova, M. Putkonen, L. Niinistö, K. Arstila, and T. Sajavaara, "Gadolinium oxide thin films by atomic layer deposition," *Journal of Crystal Growth*, vol. 285, no. 1-2, pp. 191–200, 2005.

[34] D. H. Powell, O. M. Ni Dhubhghaill, D. Pubanz et al., "Structural and dynamic parameters obtained from 17O NMR, EPR, and NMRD studies of monomeric and dimeric Gd3+ complexes of interest in magnetic resonance imaging: an integrated and theoretically self-consistent approach," *Journal of the American Chemical Society*, vol. 118, no. 39, pp. 9333–9346, 1996.

[35] A. Abragam, *Principles of Nuclear Magnetism*, Oxford University Press, Oxford, UK, 1994.

[36] A. Taborda, *Relaxometria de agentes de contraste usados em imagem por ressonância magnética nuclear*, M.S. thesis, Faculdade de Ciências da Universidade de Lisboa, 2006.

[37] M. A. Reis, P. C. Chaves, and A. Taborda, "Agate stone RAE satellites in microcalorimeter based energy fispersive spectrometry high-resolution PIXE," *X-Ray Spectrometry*, vol. 40, no. 3, pp. 141–146, 2011.